CONFERENCE PRE-PRINT

DISRUPTIONS AND MHD INSTABILITIES OBSERVED IN THE INITIAL OPERATION PHASE OF JT-60SA

T. YOKOYAMA
National Institute for Quantum Science and Technology (QST)
Ibaraki, Japan
Email: yokoyama.tatsuya@qst.go.jp

S. INOUE, S. KOJIMA, T. WAKATSUKI, H. URANO, R. SANO, Y. OHTANI, S. SUMIDA,
T. NAKANO, M. TAKECHI, A. BIERWAGE, S. NISHIMURA, and M. YOSHIDA
National Institute for Quantum Science and Technology (QST)
Ibaraki, Japan

T. SZEPESI
HUN-REN Centre for Energy Research, Institute for Atomic Energy Research
Budapest, Hungary

G. PUCELLA
ENEA, Fusion And Nuclear Safety Department
C.R. Frascati, Italy

Abstract

The characteristics of disruptions and MHD instabilities observed during the initial operation of JT-60SA have been discussed, which is beneficial for reducing the risks of damage to devices and plasma performance reduction in future tokamaks. The disruptions have been divided into three categories based on their characteristics. The most observed disruptions were vertical displacement events (VDEs). The achieved elongation without VDEs decreased as the gap between the plasma surface and the wall became large. It was also demonstrated that the MHD equilibrium control simulator (MECS) exhibits good predictability of VDE. Some disruptions occurred when the plasma equilibrium controller became no longer able to correctly capture the plasma shape and position due to non-axisymmetric magnetic perturbations, since the controller assumed axisymmetric plasma. The radiative disruptions accompanied by multiple current spikes were attributed to a sudden change in edge power balance. The sawtooth-like crashes observed in the SX emission, which obstructed the plasma current ramp-up at the low toroidal magnetic field, have been identified as the off-axis sawtooth crashes. It was thought to be the local reconnection event of the double tearing mode at the off-axis position, which was led by the off-axis EC heating. The TOPICS simulation demonstrated that the T_e profile with the off-axis peak can lead to locally reversed magnetic shear, which can cause the double tearing mode.

1. INTRODUCTION

Characteristics of disruptions and MHD instabilities observed in the initial operation of JT-60SA have been discussed to reduce the risk of impairing plasma performance or damaging the devices by such phenomena in the next operations of JT-60SA and the initial operations in the future large superconducting tokamaks such as ITER and DEMO. Since many disruptions can occur in the initial operation phase due to the lack of maturity of the operation [1, 2], it is worth investigating disruptions in the initial operation of the large superconducting tokamaks, which have difficulty controlling plasma shape and position due to high coil inductance and a limited number of PF coils.

The initial plasma operation of the JT-60SA, which is the largest superconducting tokamak in the world, was started and completed in 2023. In this phase, JT-60SA was equipped with the upper carbon divertor plates, two Gyrotrons, and the following fundamental diagnostics such as tangential CO_2 interferometer, visible spectroscopy with a tangential viewing chord, soft X-ray (SX) detector arrays, the Event Detection Intelligent Camera (EDICAM), and magnetic sensors including toroidally located Mirnov coils [3–5].

The disruptions have been divided into three categories based on their characteristics: the vertical displacement events (VDEs), disruptions caused by failure of the control, and radiative disruptions [6]. Moreover, MHD

TABLE 1. BREAKDOWN OF DISRUPTIONS IN THE INITIAL OPERATION OF JT-60SA [6].

	Total	In flat-top	In ramp-down
Disruptions	82	37	45
VDE	58	24	34
Control failure	8	6	2
Radiative	16	7	9
No disruptions	69	-	-

instabilities observed in this phase have been described in the present study, particularly the sawtooth-like crashes in the SX emission, which obstructed the plasma current ramp-up at the low toroidal magnetic field. Considering that similar MHD instability during current ramp-up limited the plasma performance in MAST-U [7], it is worth investigating the cause of this MHD instability to achieve high-performance plasma in the next operations in JT-60SA, although this MHD instability did not lead to disruption.

2. DISRUPTIONS IN THE INITIAL OPERATION OF JT-60SA

In the present study, the 82 disruptions that occurred during operations when the plasma shape and position were controlled with the CCS method and 69 discharge without disruptions have been considered. These disruptions have been categorized into three categories as shown in Table 1.

The most commonly observed disruptions were VDEs. The VDEs have been characterized by toroidally symmetrical ($n = 0$) magnetic perturbations, which corresponds to the vertical movement of plasma. The disruptions distinguished into second class named "control failure" were triggered by the failure of the control scheme due to the magnetic toroidal asymmetric perturbation. In the disruptions categorized into the third category, "radiative disruptions," plasma current slowly decreases accompanied by multiple current spikes. While the I_p decays, the spikes in SX emission and $n = 1$ magnetic perturbation were observed. Figure 1 shows distributions of Greenwald fraction $f_{GW} = \bar{n}_e/n_{GW}$, elongation κ, and OI line emission intensity when the disruption occurred for each class shown in Table 1. The class with the highest mean f_{GW} is "control failure." The VDEs have been observed with various f_{GW} and the mean value is lower than those in the other two categories, but the elongation κ is relatively higher than those in the others. The radiative disruptions were observed with relatively higher OI emission, but there were some discharges without disruptions with higher OI emission.

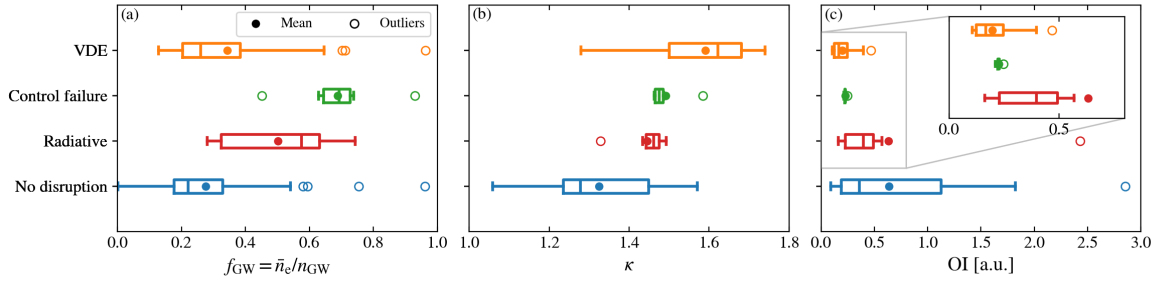

FIG. 1. Box-and-whisker plot of (a) Greenwald fraction $f_{GW} = n_e/n_{GW}$, (b) elongation κ, and (c) CI line emission for each classes shown in Table 1. In the panel (c), the close-up view is also shown. In the box-and-whisker plot, the colored vertical lines in boxes and the painted dots show the medians and means, respectively. The outlined dots show the outliers.

2.1. VDEs

It is acknowledged that the plasma vertical position is likely to be unstable with highly elongated shape, while such a shape is required to achieve high-performance plasma. In large superconducting tokamaks such as JT-60SA, the predictability of VDEs is essential because the coil inductance is high and the number of coils is limited compared to conventional conducting tokamaks.

Relationship between the plasma elongation κ and the averaged gap between plasma surface and the vacuum vessel wall δ normalized by minor radius a_p are shown in Fig. 2 (a) for VDEs and non-disruptive discharges whose Shafranov lambda $\Lambda = \beta_p + l_i/2$ were less than unity. It was revealed that the achievable κ without VDE decreased when the normalized gap became large, which is due to the weakening of the passive stabilization effect by the

wall. The dotted curve in Fig. 2 (a) is the boundary between VDE and no disruptive discharges estimated by logistic regression and expressed as $\kappa = 1.16(d/a)^{-0.273}$.

The VDE predictability of the MHD equilibrium control simulator (MECS) [8] has been evaluated by comparing the achieved κ in κ scan simulation with experiment, of which typical waveform is shown in Fig. 2 (b). Figure 2 (c) shows the comparison of achieved κ between κ-scan experiment and MECS simulations with similar δ/a_p. This result suggests that the MECS simulation can predict the achieved κ before VDE well and the relationship between κ and the normalized gap δ/a_p were well reproduced in MECS. The residual between MECS prediction and experiment is mainly due to the difference in internal inductance l_i. The open dot in Fig. 2 (c) represents the MECS simulation with l_i of 10% smaller than other simulations to make it close to the experiment. The predicted κ with smaller l_i increased and closer to experiment than the higher l_i case. Other possible cause of the difference between experiment and the MECS simulation is that the conductor model used in the MECS is not optimized, which is recognized as a remaining task.

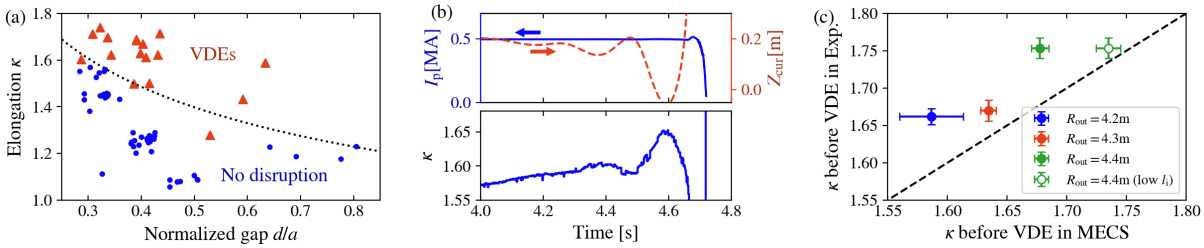

FIG. 2. (a) Relationships between κ and normalized averaged gap between plasma surface and vacuum vessel wall δ/a_p for no disruption discharges (blue dots) and VDEs (red triangles) whose Shafranov lambda were less than 1. (b) Typical waveforms of (top) plasma current I_p,vertical position of plasma current center Z_j, and (bottom) plasma elongation κ for κ-scan experiment. (c) Comparison of achieved κ before VDE between κ-scan experiment and MECS simulations with same R_{out}.

2.2. Control failure

Some disruptions have been triggered by the sudden termination of the plasma shape/position control scheme due to the non-toroidally symmetric magnetic mode. Figure 3 shows the waveform of the control failure disruption. When the $n = 1$ magnetic perturbation grew, the controllability of the plasma shape and position was lost, which is shown in the decrease in G_s, leading to the rapid vertical movement of plasma. Here, G_s is the indicator of the coil voltage availability for the plasma shape and position control [9]. This is because the controller was no longer able to correctly capture the plasma shape and position under the axisymmetric assumption due to non-axisymmetric magnetic perturbations, as all the magnetic sensors for control were located in the same poloidal cross-section in the initial operation phase. Since the magnetic sensors will be increased toroidally in the next operations, the controller will be able to ignore non-axisymmetric magnetic perturbations, allowing it to capture the plasma shape and position correctly. As a result, the control failure disruptions will be avoided in the next operations.

Figure 4 (a) shows the spectra of magnetic and SX fluctuations between the vertical dashed lines in Fig. 3. The SX fluctuations in the most of lines have peaks at the same frequency of 700 Hz as the magnetic fluctuation. The SX signal has been reconstructed using the Tikhonov-Philips regularization method [10], one of the tomography techniques, to show that the phases of 700 Hz components for each radial position are shown in Fig. 4 (b). The phase inversion is seen at $\rho \sim 0.45$, which indicates $n = 1$ tearing mode structure existed here.

2.3. Radiative disruptions

Radiative disruptions were characterized by the slow current decay with multiple spikes, which can bee seen in Fig. 5. The spikes were also observed in SX emissions and the $n = 1$ mode grew before each spike. These disruptions are thought to be triggered by an imbalance of heating power and radiative loss at the plasma edge because they occurred just after the ECH stopped and/or in high particle supply conditions. When the current decay started, the spikes were observed in the visible spectroscopy signals. These spikes correspond to the X-point radiator (XPR) passing across the line of sight, which appeared at the upper X-point and moved downward by ∇B drift, observed by the EDICAM [5]. The existence of XPR is the evidence that the plasma is cooled from edge.

As shown in the bottom panel of Fig. 5, the spikes in the SX signal had inverted directions between the core and edge channels, and the inverse position (channel) was moving toward the core. This implies that the cooling front was penetrating while the current slowly decayed, and the spikes occurred when the cooling front crossed the resonance surface and the plasma current and temperature were locally flattened.

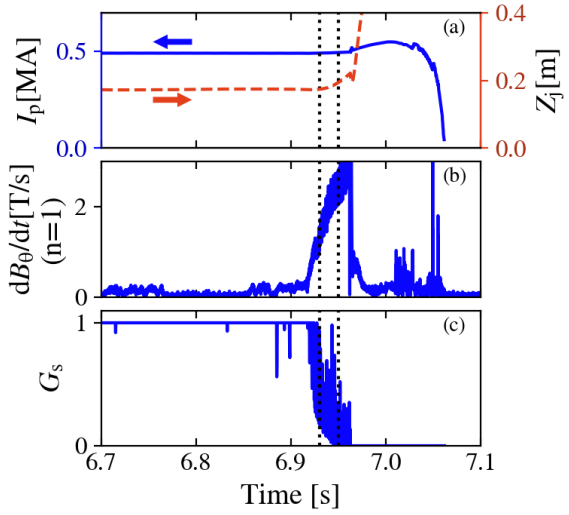

FIG. 3. Typical waveforms for control failure disruption. From top to bottom, plasma current I_p, and vertical position of plasma current center Z_j, $n = 1$ magnetic perturbation amplitude dB_θ/dt, and the indicator of the coil voltage availability for the plasma shape and position G_s.

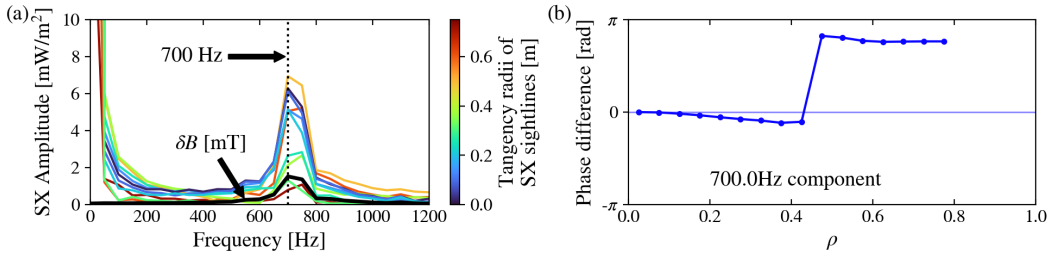

FIG. 4. (a) Spectra of the magnetic fluctuation and the SX emission fluctuations in each line of sight of the SX detector array. (b) The phase of 700 Hz component of reconstructed SX emission density using the Tikhonov-Philips regularization method [6].

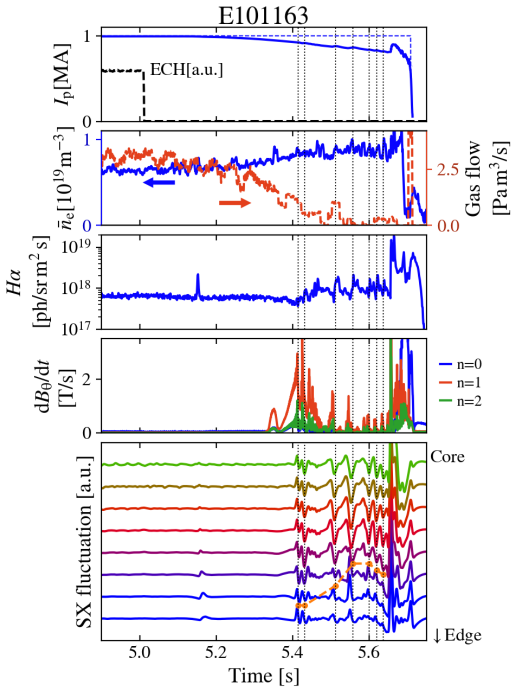

FIG. 5. Typical waveform of radiative disruption. In the bottom panel, SX emission of each channel of the detector array with 10–500 Hz band pass filter are shown with the position of spike inversion in orange-dashed line. The dashed vertical lines represent the timing of I_p spikes.

3. SAWTOOTH-LIKE CRASHES IN CURRENT RAMP-UP AT LOW TOROIDAL MAGNETIC FIELD

In addition to the $n = 1$ tearing mode and the local flattening by cold front penetration described above, sawtooth-like events have been observed in the initial operation phase of JT-60SA. The present study focus on the sawtooth-like crashes among in the plasma start-up experiment in toroidal field B_t of 1.7 T, which is lower than its usual value of 2.04 T, among these MHD instabilities. Fig. 6 shows the typical waveforms at B_t =1.7 T with and without sawtooth-like crash. In these discharges, EC heating was used to assist plasma current ramp-up under the limitation of CS voltage. The sawtooth-like crash appeared in SX emission in eight of nine low-B_t discharges and the current ramp-up was disturbed at the same time. This event did not directly caused the disruptions but can reduce plasma performance like the MHD instability named internal reconnection event (IRE) observed in the current ramp-up in MAST-U [7].

According to Fig. 7 (b) showing the sawtooth-like crash in line-integrated SX emissions, the phase of the crashes are inverted between the channels that don't seeing the plasma center, and the amplitude of these channels are larger than those if the core channels. Note that the lines of sight of the SX detector array are described in Fig. 7 (a). These observations indicate that the sawtooth crash occurred off-axis region, so that this instability was identified as the off-axis sawtooth (or annular crash) [11, 12]. The off-axis sawtooth disappeared and the plasma current ramp-up was no longer disturbed after the B_t was set to 2.04 T.

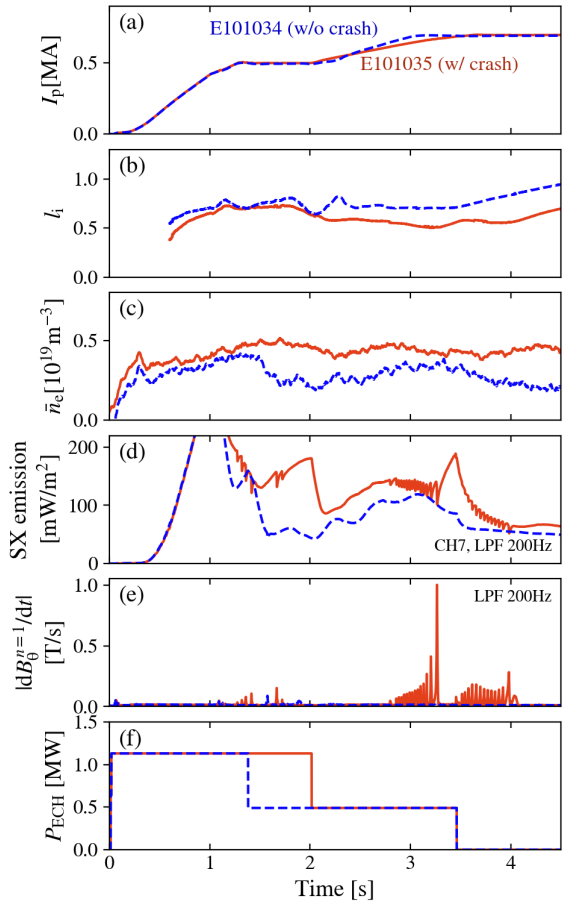

FIG. 6. (a) Plasma current I_p, (b) internal inductance l_i, (c) line-averaged density $\bar{n}_e$, (d) line-integrated SX emission, (e) $n = 1$ magnetic perturbation amplitude dB_θ/dt, and (f) EC heating power for (red) with and (blue) without off-axis sawtooth discharges.

Fig. 7 (c) shows the close-up of the precursor perturbation of the off-axis sawtooth. The precursor has frequency of about 1 kHz and its phase was inversed on either side of the inverse position of the sawtooth, which suggests that the off-axis sawtooth is the magnetic reconnection event between two magnetic islands, double tearing mode (DTM), which is known as the main cause of the off-axis sawtooth. Consequently, the possible mechanism of this off-axis sawtooth is that the current ramp-up while T_e profile had a peak at off-axis due to off-axis EC heating,

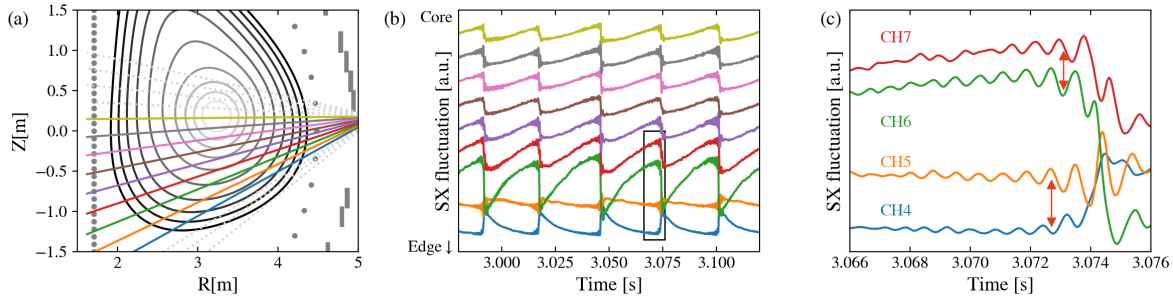

FIG. 7. (a) The lines of sight of the SX detector overlapping on the flux surface, (b) the fluctuation components of the line-integrated SX emissions, and (c) a close up of the boxed area in (b). The line colors are corresponding to each other.

leading to the current profile with an off-axis peak, in other words, q profile with locally inverted shear at the off-axis position. This is consistent with the knowledge that the DTMs are often observed in the reversed magnetic shear configurations.

Figure 8 shows that the off-axis sawtooth were observed when the high EC heating power of above 1 MW were injected with off-axis resonance at around $\rho \sim 0.6$, which was the common feature of B_t =1.7 T discharges. When B_t =2.04 T, the EC resonance position was more close to the plasma center and the off-axis sawtooth were not observed when the EC heating power was above 1.0 MW. In these discharges, the second harmonic X-mode wave of 110 GHz were used for EC heating. This suggests that the temperature profile has a peak at off-axis position when off-axis sawtooth was observed, which supports the possible mechanism of the off-axis sawtooth described above.

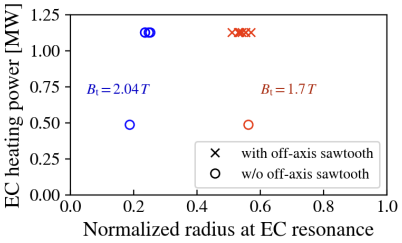

FIG. 8. The relationship between the EC resonance position and EC heating power at beginning of the plasma current ramp-up from 0.5 MA *in (red)* B_t =1.7 T *and (blue)* 2.04 T *discharges. The crosses and circles represent discharges with and without the off-axis sawtooth, respectively.*

The q profile when T_e profile has an off-axis peak was estimated using the integrated simulation code TOPICS [13], since the q and T_e profiles were not measured in the initial operation phase of the JT-60SA. Figure 9 shows the results of the TOPICS simulation with given n_e and T_e profiles. When the T_e profile has a peak at ρ = 0.6, the safety factor q profiles have a local minimum at $\rho \sim 0.7$, which can lead the double tearing mode at the off-axis region. Moreover, the local minimum q becomes smaller and the inverted magnetic shear inside the local minimum becomes steeper when the peak T_e becomes higher.This result supports the possible mechanism of the off-axis sawtooth in the B_t =1.7 T experiments. In contrast, the q profiles with center-peaked T_e profiles were almost monotonous.

4. SUMMARY

The present research aims to clarify the characteristics of disruptions and MHD instabilities observed in the initial operation of the JT-60SA to reduce the risk of impairing plasma performance or damaging the devices in future tokamak operations.

The disruptions have been classified into three categories: VDEs, control failure, and radiative disruptions, and the possible mechanisms and the conditions under which the disruptions are likely to occur were discussed for each category. Especially, it has been shown that the MECS simulation has good predictability for the achievable κ without VDEs. It is also important to eliminate the effect of non-axisymmetric magnetic perturbations for stable control of plasma shape and position. Moreover, sudden loss of power balance at the plasma edge, which was mainly triggered by termination of EC heating, can cause radiative disruption. The above discussions can

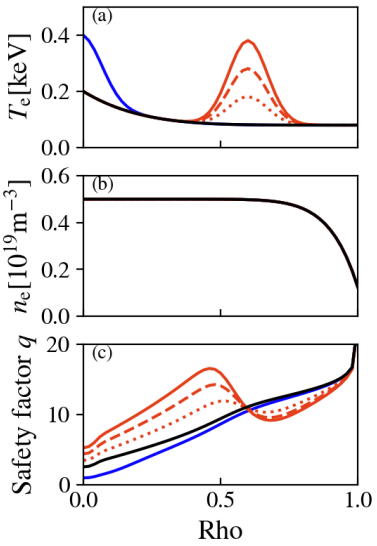

FIG. 9. Profiles of (a) electron temperature T_e, (b) electron density n_e, and (c) safety factor q of the TOPICS simulation results.

contribute to identifying disruptions likely to occur in the early operations of future large tokamaks like ITER and DEMO.

The sawtooth-like crashes in the SX emission during the plasma current ramp-up at the low toroidal magnetic field condition have been identified as the off-axis reconnection event of double tearing mode. This instability was possibly caused by the off-axis peak in T_e profile due to the off-axis EC heating. It was demonstrated that the safety factor profiles with locally inverted magnetic shear can appear with such the T_e profiles. It is worth pointing out that the plasma performance may be reduced by MHD instabilities such as the off-axis sawtooth, even in the initial phase of the tokamak operation in which the surface safety factor is high.

ACKNOWLEDGEMENTS

JT-60SA was jointly constructed and is jointly funded and exploited under the Broader Approach Agreement between Japan and EURATOM.

REFERENCES

[1] DE VRIES, P. C. et al., Statistical analysis of disruptions in JET, Nuclear Fusion **49** 5 (2009) 055011.

[2] DE VRIES, P. C. et al., Survey of disruption causes at JET, Nuclear Fusion **51** 5 (2011) 053018.

[3] YOSHIDA, M. et al., Overview of plasma operation and control studies in the first plasma campaign of JT-60SA, Plasma Physics and Controlled Fusion **67** 6 (2025) 065010.

[4] SASAO, H. et al., Development of CO2 laser interferometer/polarimeter system in JT-60SA, Journal of Instrumentation **11** 02 (2016) C02082.

[5] SZEPESI, T. et al., Wide-angle visible video diagnostics for JT-60SA utilizing EDICAM, Fusion Engineering and Design **153** (2020) 111505.

[6] YOKOYAMA, T. et al., Characteristics of disruptions observed in the initial operation phase of JT-60SA, Nuclear Fusion **64** 12 (2024) 126031.

[7] BERKERY, J. W. et al., Operational space and performance limiting events in the first physics campaign of MAST-U, Plasma Physics and Controlled Fusion **65** 4 (2023) 045001.

[8] MIYATA, Y. et al., Study of Plasma Equilibrium Control for JT-60SA using MECS, Plasma and Fusion Research **9** (2014) 3403045.

[9] INOUE, S. et al., Development of JT-60SA equilibrium controller with an advanced ISO-FLUX control scheme in the presence of large eddy currents and voltage saturation of power supplies, Nuclear Fusion **61** 9 (2021) 096009.

[10] IWAMA, N. et al., Phillips–Tikhonov regularization of plasma image reconstruction with the generalized cross validation, Applied Physics Letters **54** 6 (1989) 502–504.

[11] CHANG, Z. et al., Off-Axis Sawteeth and Double-Tearing Reconnection in Reversed Magnetic Shear Plasmas in TFTR, Physical Review Letters **77** 17 (1996) 3553–3556.

[12] BURATTI, P. et al., MHD activity in FTU plasmas with reversed magnetic shear, Plasma Physics and Controlled Fusion **39** 12B (1997) B383.

[13] HAYASHI, N. et al., Advanced tokamak research with integrated modeling in JT-60 Upgrade, Physics of Plasmas **17** 5 (2010) 056112.